Sustainable Energy & Fuels

Interdisciplinary research for the development of sustainable energy technologies

Accepted Manuscript

This article can be cited before page numbers have been issued, to do this please use: L. Guo, K. Miyatake, F. Xian, F. Liu, A. M. A. Mahmoud, V. Yadav and C. Y. Wong, *Sustainable Energy Fuels*, 2025, DOI: 10.1039/D5SE00825E.

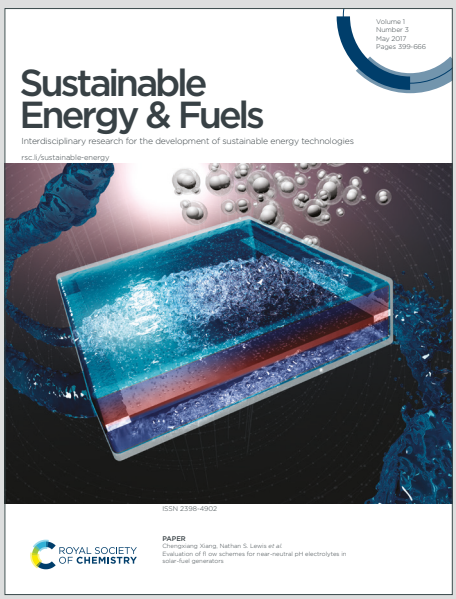

View Article Online
DOI: 10.1039/D5SE00825E

Enhanced Performance of All-Solid-State Rechargeable Air Batteries with Redox-Active Naphthoquinone-Based Polymer Electrode

Lin Guo[a], Kenji Miyatake*[a,b,c], Fang Xian[a], Fanghua Liu[a], Ahmed Mohamed Ahmed Mahmoud[a], Vikrant Yadav[a], Chun Yik Wong[a]

[a]Clean Energy Research Center, University of Yamanashi, Kofu, Yamanashi 400-8510, Japan.

[b]Hydrogen and Fuel Cell Nanomaterials Center, University of Yamanashi, Kofu, Yamanashi 400-8510, Japan

[c]Department of Applied Chemistry, Waseda University, Tokyo 169-8555, Japan.

*Corresponding author

E-mail address: miyatake@yamanashi.ac.jp (Kenji Miyatake)

View Article Online
DOI: 10.1039/D5SE00825E

Abstract

All-solid-state rechargeable air batteries (SSABs) have emerged as a promising next-generation battery technology, eliminating the need for liquid electrolytes and reducing the reliance on metal-based electrode materials, while mitigating bulky design issues such as excessive mass and size. Herein, we propose an SSAB that uses a novel redox-active polymer containing the naphthoquinone moiety (PPNQ) as the negative electrode material and evaluate its electrochemical performance. The SSAB-PPNQ cell exhibited superior rate capability and charge/discharge cycle stability compared to SSABs utilizing small organic molecules, owing to the enhanced structural stability and redox reversibility of PPNQ. The reduced dissolution and/or possible degradation during repeated charge/discharge cycles enhanced the rate properties (84% retention of its discharge capacity at 100 C) and cyclability (98% retention of its charge/discharge capacities over 100 cycles) of the SSAB-PPNQ cell, highlighting the potential of PPNQ redox-active polymer as a promising candidate for high-performance SSABs.

View Article Online
DOI: 10.1039/D5SE00825E

With increasing demand for sustainable and high-performance energy storage systems, organic electrode materials have emerged as promising candidates for secondary batteries due to their environmental benignity, structural diversity, and tunable redox properties. In particular, organic air batteries, which utilize redox-active organic molecules as the negative electrode material and ambient air as the positive reactant, offer great potential for light-weight, cost-effective, and eco-friendly energy storage devices.[1, 2, 3] Compared to the conventional metal-air batteries which employ metal-based (Li, Na, Zn, etc.) negative electrodes, use of organic-based negative electrodes avoid issues such as dendrite formation and parasitic side reactions, while providing greater molecular design flexibility, redox reversibility, and water stability. [4, 5, 6] For example, a π-conjugated N-heteroaromatic phenazine derivative (NHCC) was previously used as the active negative electrode material in an organic-air battery, exhibiting a high cell voltage of 1.6 V and lifetime of 30,000 charge/discharge cycles when coupled with aqueous electrolyte (4 M KOH and 10 M KCF_3SO_3).[7] Additionally, an air battery using 1,8-dihydroxyanthraquinone-substituted poly(allyl amine) (PDHA) as the negative electrode material and aqueous H_2SO_4 as the electrolyte exhibited a discharge capacity of 140 mAh g^{-1}, with excellent cyclability (>97% retention of its discharge capacity over 500 charge/discharge cycles) and a high rate capability up to 120 ^oC.[8] A redox-active donor-acceptor conjugated microporous polymer (AQ-CMP) containing anthraquinone and benzene served in negative electrode in air battery which demonstrated a specific capacity of 202 mAh g^{-1} (96% of theoretical capacity) at 2 A g^{-1}, excellent rate capability (58% capacity retention at 20 A g^{-1}), and ca. 100% capacity retention over 60000 charge/discharge cycles in 6 M KOH solution.[9] Despite the encouraging results, the use of liquid electrolytes provided those organic–air batteries with some drawbacks such as electrolyte leakage, increased weight, and limited compatibility with miniaturized or flexible devices. To overcome those limitations, combination of solid polymer electrolyte with organic negative electrodes seems a promising direction, particularly for next-generation compact energy storage systems.

View Article Online
DOI: 10.1039/D5SE00825E

We recently developed organic SSABs using 2,5-dihydroxy-1,4-benzoquinone (DHBQ) or its polymeric counterpart, poly(2,5-dihydroxy-1,4-benzoquinone-3,6-methylene) (PDBM), as the negative electrode material and a proton-conductive Nafion™ membrane as the solid electrolyte.[10] The batteries were operable with an open circuit voltage (OCV) of 0.80 V. Notably, the SSAB-PDBM cell achieved a higher discharge capacity (176.1 mAh g^{-1}) than the SSAB-DHBQ cell (29.7 mAh g^{-1}) and retained 78% of its capacity over 30 charge/discharge cycles, highlighting the promising potential of polymeric redox-active molecules in SSABs. More recently, we fabricated an SSAB using 1,4-naphthoquinone (NQ) as the negative electrode material and a less gas-permeable aromatic ionomer–based proton-conductive membrane (SPP-QP) as the solid electrolyte.[11] The SPP-QP membrane, with an ion exchange capacity (IEC) of 3.1 mmol g^{-1}, exhibited proton conductivities of 0.157 S cm^{-1} at 80 °C and 0.077 S cm^{-1} at 40 °C under 80% relative humidity (RH) (Figure S1), both of which were higher than those of the commercial Nafion 212 membrane (0.100 S cm^{-1} at 80 °C and 0.066 S cm^{-1} at 40 °C). The results indicate that the SPP-QP membrane possesses sufficient proton conductivity to support effective proton transport in the SSAB configuration. The SSAB-NQ cell exhibited an OCV of 1.06 V and prolonged charge/discharge cyclability, retaining 88% of its capacity over 100 charge/discharge cycles and >98% of its Coulombic efficiency (CE) over 135 cycles. These results prompted us to design a novel redox-active polymer containing the NQ moiety (PPNQ) as the negative electrode material in SSABs. In the present study, the synthesis, electrochemical properties, and SSAB performance of PPNQ were investigated and compared to those of our previously reported SSABs.

The DPNQ monomer was synthesized through the bromination of NQ, followed by reaction with 4-chlorophenylboronic acid via Pd(0)-catalyzed cross-coupling reaction (Figure 1a) in a total yield of 47%. The chemical structure of DBNQ and DPNQ was confirmed by ^{1}H and ^{13}C nuclear magnetic resonance (NMR) spectra (Figure 1b and c). The PPNQ polymer was then synthesized through the polymerization of the DPNQ

View Article Online
DOI: 10.1039/D5SE00825E

monomer via Ni(0)-mediated polycondensation reaction, whose structure was also confirmed by ^{1}H NMR spectrum (Figure 1d). The resulting PPNQ polymer was soluble in N,N-dimethylformamide (DMF), N,N-dimethylacetamide (DMAc), and dimethyl sulfoxide (DMSO). The molecular weight of the PPNQ was M_w = 3.26 kDa and M_n = 2.20 kDa with a narrow polydispersity index (M_w/M_n = 1.49).

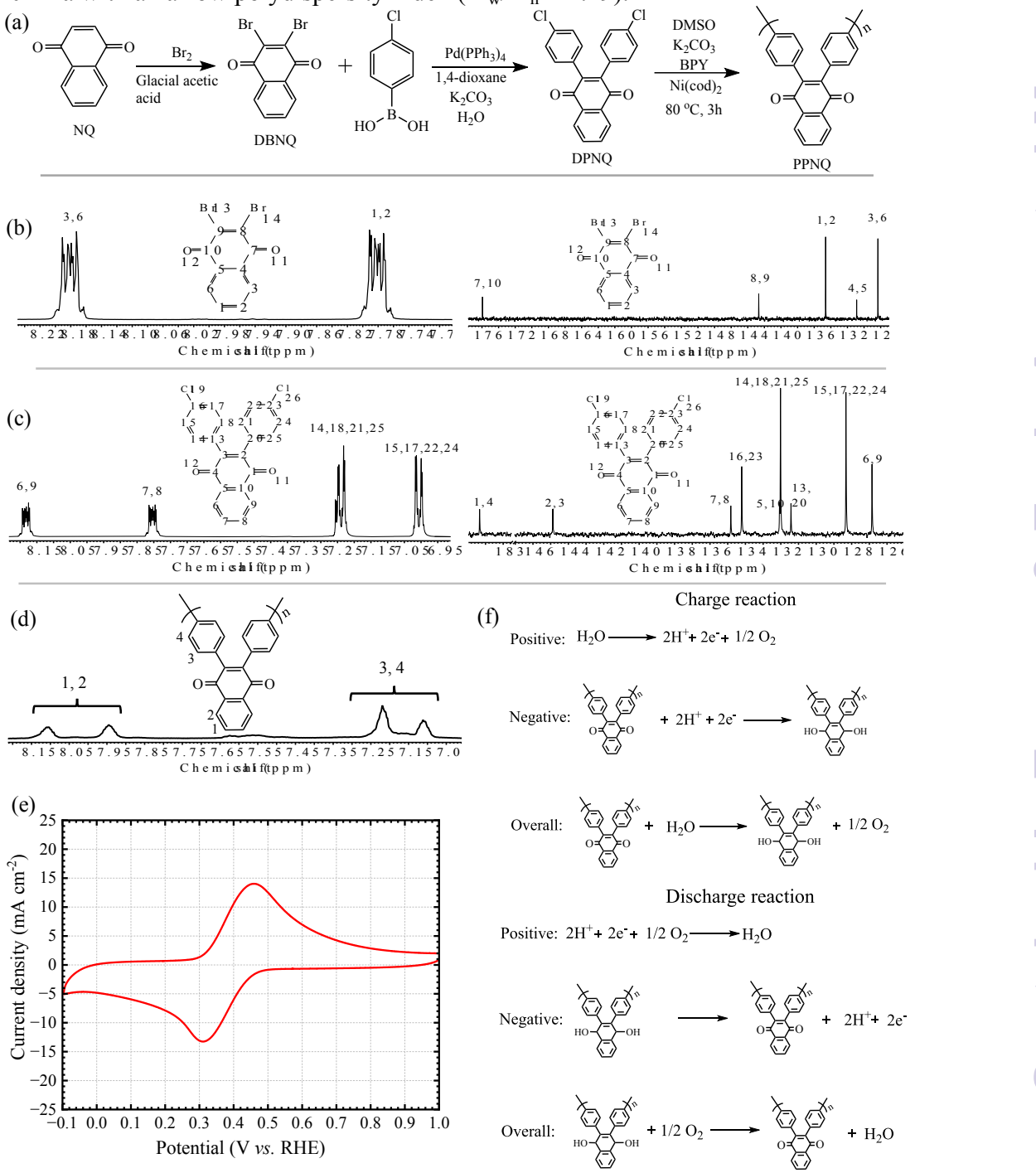

View Article Online
DOI: 10.1039/D5SE00825E

Figure 1. (a) Synthetic scheme of DBNQ and DPNQ monomers and PPNQ polymer. ^{1}H (left) and ^{13}C (right) NMR spectra of (b) DBNQ and (c) DPNQ in $CDCl_3$ at room temperature. ^{1}H NMR spectra of PPNQ polymer in $DMSO_{-d6}$ at room temperature. (e) CV curves of the SSAB-PPNQ cell scanned at 20 mV s^{-1} (40°C and 80% RH) for the negative electrode. (f) Electrode and overall reactions during charging and discharging.

A catalyst-coated membrane (CCM) containing platinum/carbon (Pt/C) as the positive electrode catalyst and PPNQ as the redox-active negative electrode material was prepared and assembled into a cell (see Supplementary Information for details). The cross-sectional scanning electron microscopy (SEM) images of the freshly prepared CCM are shown in Figure S2a–c. The positive and negative electrode inks were uniformly sprayed onto both sides of the SPP-QP membrane (ca. 60 μm-thick), forming consistent electrode layer with the thicknesses of ca. 20 and 100 μm, respectively. No significant aggregated clusters were observed in the magnified images for electrodes, indicating the successful fabrication of uniform CCM. Sulfur intensity in the EDS analysis (Figure S2g) as a measure of the sulfonic acid group density revealed that the sulfonic acid content in the SPP-QP membrane (ca. 85%) was more than four times higher than that in the negative electrode layer (ca. 20%). The lower sulfonic acid density combined with the greater thickness of the negative electrode layer suggests that proton transport was probably limited within the negative electrode compared to that in the SPP-QP membrane. Prior to charging and discharging the SSAB, the cyclic voltammetry (CV) curve of the negative electrode was measured at 80% relative humidity (RH). Compared to the CV curve of the monomeric NQ-based negative electrode reported in our previous paper, which exhibited major redox peaks at ca. 0.40 and 0.48 V with minor peaks at 0.28 and 0.52 V, the SSAB-PPNQ cell displayed a single set of distinct redox peaks at 0.46 and 0.31 V (Figure 1e). The results suggested the occurrence of a one-step two-electron transfer process during the hydroquinone/quinone redox reaction in PPNQ. NQ utilization in the SSAB-PPNQ

View Article Online
DOI: 10.1039/D5SE00825E

cell (based on the charge of the reduction peak divided by the number of moles of the NQ moiety in PPNQ loaded in the electrode, assuming a two-electron redox reaction) was calculated to be 17.0%, which was slightly higher than that in the SSAB-NQ cell (16.5%, measured at 100% RH). The improved NQ utilization in the SSAB-PPNQ cell compared to the SSAB-NQ cell indicated that the affinity of polymeric PPNQ for the hydrophilic proton-conducting polymer (Nafion^{TM}) was potentially better than that of monomeric NQ. Similar results were obtained with DHBQ. Additionally, the CV curve of the PPNQ negative material was measured in an aqueous acidic solution (0.05 M sulfuric acid) at room temperature as shown in Figure S3. Distinct redox peaks were observed at 0.41 and 0.38 V with a narrow potential separation of 0.03 V compared to 0.15 V observed in the SSAB. The results indicate a more reversible redox reaction in the aqueous electrolyte due to the enhanced proton supply. Furthermore, the utilization of NQ in the aqueous electrolyte reached 83.4%, which was more than four times higher than that in the SSAB. The limited proton supply in the solid-state lowered the utilization of the redox-active material in the negative electrode. Electrochemical impedance spectroscopy (EIS) of the SSAB-PPNQ cell was conducted after the CV measurement, and the results are presented as a Nyquist plot in Figure S4. The plot exhibited two distinct semicircles in the high- and mid-frequency regions. The small semicircle at high frequency was attributed to the interfacial resistance and contact impedance between the solid electrolyte and the electrodes. The larger semicircle at mid frequency was ascribed to the charge-transfer resistance associated with the proton-coupled redox reactions occurring at both electrodes. The energy storage mechanism of the SSAB-PPNQ cell involves proton-coupled redox reactions at both electrodes as illustrated in Figure 1f. During the charging, the PPNQ negative electrode is reduced by accepting two electrons and two protons per quinone unit forming hydroquinone. The protons are originated from water splitting at the positive electrode, where water molecules are oxidized to release protons and oxygen. During the discharging, the hydroquinone units in the PPNQ are oxidized back to quinone, releasing electrons and protons. Meanwhile, the oxygen at the positive electrode is reduced to water

View Article Online
DOI: 10.1039/D5SE00825E

with electrons and protons, completing the redox cycle. The charging/discharging curves of the SSAB-PPNQ cell obtained at a constant current density of 0.23 mA cm^{-2} (at 3.9 C rate) are illustrated in Figure 2. During charging, the potential of the positive electrode (where the water oxidation reaction occurred to generate oxygen) (Figure 2a) initially increased from ca. 0.97 to 1.05 V and then gradually increased to ca. 1.14 V. In the final stage of charging, the potential increased rapidly to ca. 1.23 V, which was attributed to the accumulation of oxygen generated on the electrode surface causing mass transport overpotential.[12] The potential of the negative electrode (where PPNQ was reduced) (Figure 2b) rapidly decreased from ca. 0.79 to 0.40 V and then gradually decreased to 0 V, at which point charging was terminated to avoid the occurrence of the hydrogen evolution reaction (HER) (or proton reduction reaction). Accordingly, the cell voltage (Figure 2c) rapidly increased from ca. 0.18 to 0.64 V and then gradually increased to ca. 1.23 V, mostly dominated by the negative electrode. The charge capacity was 74.4 mAh g^{-1}, from which the PPNQ utilization was calculated to be 40%, which was 23% higher than that calculated from the CV curve. These results suggested that more PPNQ molecules participated in the redox reaction under dynamic than static conditions. During discharging, the potential of the positive electrode (where oxygen was reduced to produce water) (Figure 2a) rapidly decreased from ca. 0.95 to 0.88 V and then remained nearly constant until the end of the discharging process, whereas the potential of the negative electrode (where PPNQ was oxidized) initially quickly increased from ca. 0.23 to 0.30 V and then gradually increased to ca. 0.45 V, followed by another sharp rise to ca. 0.88 V (Figure 2b). The OCV of the SSAB-PPNQ cell (0.73 V) was lower than that of our previous SSABs using DHBQ, NQ, and PE-AQ, an anthraquinone derivative,[13] (ca. 0.80, 1.10, and 1.10 V, respectively, when operated at 100% RH (Figure 2c). The lower OCV of the SSAB-PPNQ cell compared to previous SSABs was mainly attributed to the higher redox potential and the large redox peak separation (or electrochemical irreversibility) of the PPNQ redox reaction, in addition to the lower but more practical RH used in this study compared to the fully humidified conditions adopted in previous studies (80% vs. 100%

View Article Online
DOI: 10.1039/D5SE00825E

RH). In fact, the OCV of the SSAB-NQ cell decreased to ca. 1.05 V when operated at 80% RH. As discharging proceeded, the cell voltage of the SSAB-PPNQ cell rapidly decreased to 0.58 V and then gradually decreased to ca. 0.55–0.45 V, presenting a somewhat higher nominal cell voltage (near the plateau cell voltage during discharging) than the SSAB-DHBQ and SSAB-NQ cells (ca. 0.50–0.30 and 0.40–0.24 V, respectively) but a lower nominal cell voltage than the SSAB-PE-AQ cell (ca. 0.70–0.60 V). Similar to the charging process, the cell voltage during discharging was dominated by the negative electrode. The discharge capacity of the SSAB-PPNQ cell (63.1 mAh g^{-1}) was higher than that of the SSAB-DHBQ cell (29.7 mAh g^{-1}), which was attributed to the instability of the negative electrode, but it was lower than those of the SSAB-NQ and SSAB-PE-AQ cells (83.6 and 99.9 mAh g^{-1}, respectively). Compared to the SSAB-NQ cell, which exhibited a discharge capacity of 50.0 mAh g^{-1} at 80% RH, the SSAB-PPNQ cell was more capacitive. The CE of the SSAB-PPNQ cell (85%) was lower than those of the SSAB-DHBQ, SSAB-NQ, and SSAB-PE-AQ cells (ca. 100%, 87% and 100%, respectively), which was presumably caused by the limited redox reactions of PPNQ owing to electrochemical irreversibility under lower humidity (80% RH) conditions. The charging/discharging curves of the SSAB-PPNQ cell at lower constant current densities of 0.06 mA cm^{-2} (1 C rate) and 0.03 mA cm^{-2} (0.5 C rate) are shown in Figure S5. Compared to the performance at 3.9 C, the increased charge/discharge capacities (73.5/67.0 mAh g^{-1} at 1 C and 81.2/78.7 mAh g^{-1} at 0.5 C) and improved CEs (91% at 1 C and 97% at 0.5 C) indicate that lower C rates effectively improved the proton supply and redox kinetics of PPNQ in the solid-state.

View Article Online
DOI: 10.1039/D5SE00825E

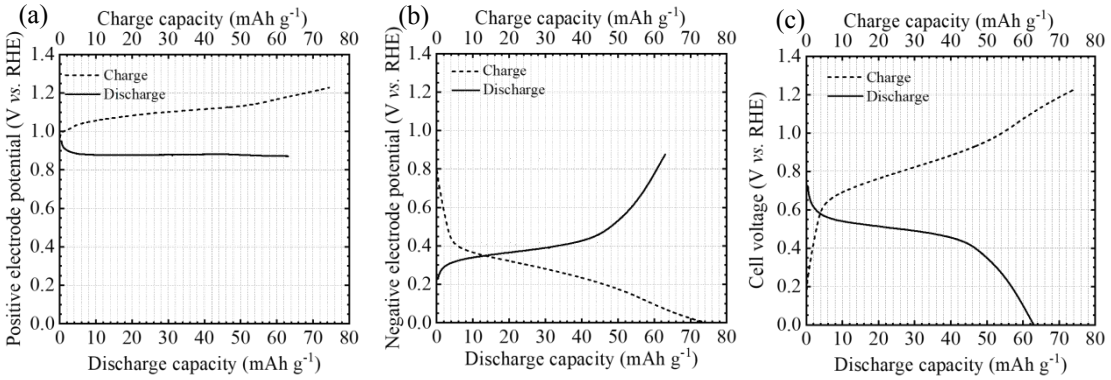

Figure 2. Charging/discharging curves of the SSAB-PPNQ cell measured at a current density of 0.23 mA cm^{-2}: (a) positive electrode potential, (b) negative electrode potential, and (c) cell voltage.

Based on the abovementioned discharge capacity, the C rate was determined. The rate characteristics were evaluated while increasing the discharge rate from 4 to 100 C (or a current density from 0.24 to 5.87 mA cm^{-2}), while the charge rate was maintained at 4 C. The discharging curves at different C rates are summarized in Figure 3a–c (see Figure S6 for the charging curves). The initial positive (Figure 3a) and negative (Figure 3b) electrode potentials remained nearly constant at all discharge C rates, at ca. 0.92 and 0.20 V, respectively, resulting in the same OCV of ca. 0.72 V for the SSAB-PPNQ cell (Figure 3c). The discharge capacity of the SSAB-PPNQ cell decreased from 68.4 to 57.4 mAh g^{-1} from 4 to 100 C, retaining 84% of its discharge capacity at 100 C, which was superior to that of the SSAB-NQ cell (79% retention of its discharge capacity when operated at 100 C rate and 100% RH). The final potential (at which discharging was terminated) of negative electrode decreased from ca. 0.77 to 0.72 V from 4 to 100 C, retaining 94% of its initial value at 100 C. Given that the positive electrode potential of the SSAB-PPNQ, SSAB-NQ, and SSAB-PE-AQ cells exhibited a similar dependence on the discharge rate, the rate characteristics of the discharge capacity were mostly dominated by the negative

View Article Online
DOI: 10.1039/D5SE00825E

electrode. The negative electrode potential of the SSAB-NQ cell was initially ca. 0.19 V, and the final potential decreased from ca. 0.83 to 0.71 V from 4 to 100 C, retaining 86% of its initial value at 100 C, which was inferior to that of the SSAB-PPNQ cell. The CE of the SSAB-PPNQ cell decreased from 84% to 81% from 4 to 100 C (Figure 3d), which was lower than those of the SSAB-NQ and SSAB-PE-AQ cells (100% to 91% and 96% to 93%, respectively, when operated at 100% RH).

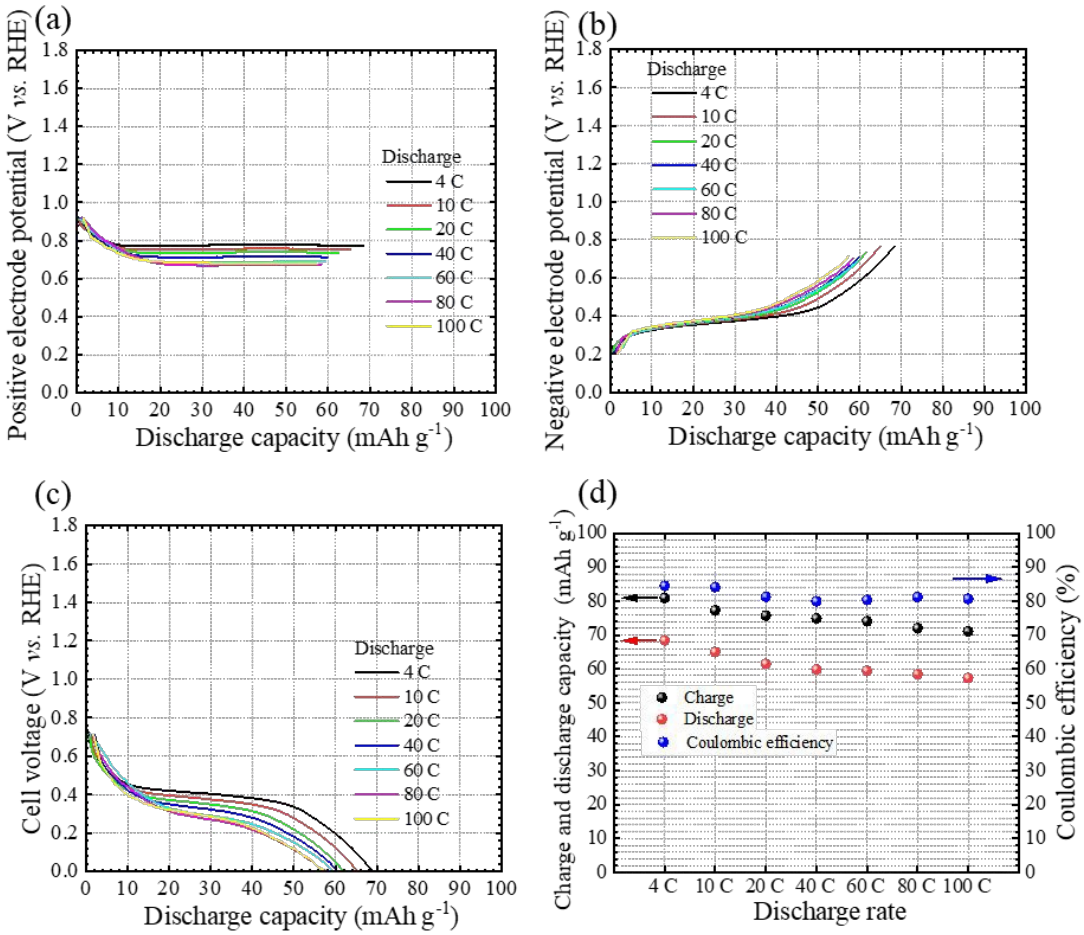

Figure 3. Discharging curves of the SSAB-PPNQ cell: (a) positive electrode potential, (b) negative electrode potential, (c) cell voltage, and (d) Coulombic efficiency measured at 4, 10, 20, 40, 60, 80, and 100 C rates (or current densities of 0.24, 0.59, 1.17, 2.35, 3.53, 4.70 and 5.87 mA cm^{-2}).

View Article Online
DOI: 10.1039/D5SE00825E

The SSAB-PPNQ cell was charged and discharged at a constant current density of 0.88 mA cm^{-2} (or 15 C rate) at 80% RH for 100 cycles, with a restart every 20 cycles, and the charging/discharging curves are presented for every 10 cycles (Figure 4a–c). Although the charging/discharging curves of the electrodes and cell (Figure 4a–c) in the 1st cycle were similar to those obtained at a lower current density (0.23 mA cm^{-2} or 3.9 C rate, Figure 2), the overpotentials at both electrodes were slightly higher, resulting in slightly lower charge and discharge capacities of 67.0 and 57.6 mAh g^{-1} respectively (vs. 74.4 and 63.1 mAh g^{-1}, respectively, in Figure 2). The rate characteristics are discussed in more detail above. During the initial four cycles, the charge and discharge capacities gradually decreased from 67.0 and 57.6 mAh g^{-1} to 62.8 and 58.7 mAh g^{-1} from the 1st to the 4th cycles, respectively (Figure S7). Thereafter, the charging/discharging curves remained nearly unchanged for up to 100 cycles, indicating the excellent cycling stability of the SSAB-PPNQ cell. At the 100th cycle, the charge and discharge capacities were 61.3 and 57.5 mAh g^{-1}, respectively, accounting for 98% remaining compared to those of the 4th cycle (Figure 4d). The CE of the SSAB-PPNQ cell remained nearly constant, at 93% over 100 cycles, which was slightly lower than that of the SSAB-NQ cell (>98% over 100 cycles at 100% RH). Nevertheless, the SSAB-PPNQ cell exhibited superior cycle stability compared to the SSAB-NQ cell, as the discharge capacity of the latter declined from 81.7 to 73.6 mAh g^{-1} over 100 cycles, with ca. 90% retention of its discharge capacity. The improved stability of the SSAB-PPNQ cell in both rate performance and cycling test (as summarized in Table S3) compared to the SSAB-NQ cell was partly attributable to the polymeric structure of PPNQ, which stabilized the negative electrode without dissolution and/or decomposition. The CV curve of the negative electrode after 100 cycles was nearly identical to that of the pristine one, with a slightly higher redox-active material utilization (18% vs. 17%) (Figure 4e), further proving the excellent stability of PPNQ in the electrode. However, a sharp peak was observed at ca. −0.1 V in the cycled CV curve in the negative-going scan, indicating that

View Article Online
DOI: 10.1039/D5SE00825E

HER was more likely to occur in the aged electrode.[14] The EIS spectrum (Figure S4) of the cycled SSAB-PPNQ cell showed only slightly lower Z′ value (ca. 1.13 Ω) compared to the pristine cell (ca. 1.16 Ω), confirming the electrochemical stability of the electrode components. The cycled SSAB-PPNQ cell under fully humidified conditions (100% RH) demonstrated a more pronounced redox peak in the CV curve and higher redox-active material utilization compared to operation at 80% RH (20% vs. 18%) (Figure S8). The charging/discharging curves at 100% RH remained similar to those at 80% RH, and the charge and discharge capacities were larger, ca. 90 and 72 mAh g^{-1} at 0.23 mA cm^{-2} (at 3.4 C rate) (Figure S9) and 68 and 64 mAh g^{-1} at 1.02 mA cm^{-2} (at 15 C rate) (Figure S10), respectively, suggesting enhanced capacity at higher humidity. The charging/discharging curves were stable over 10 cycles. The aged CCM recovered from the cell was analyzed by SEM to examine the cross-sectional morphologies of the positive and negative electrodes (Figure S2d–f). The images revealed that the morphology and thickness of both electrodes remained unchanged and nearly identical to those of the fresh CCM with no evidence of particle aggregation, indicating stability of the electrode components during the cycle test.

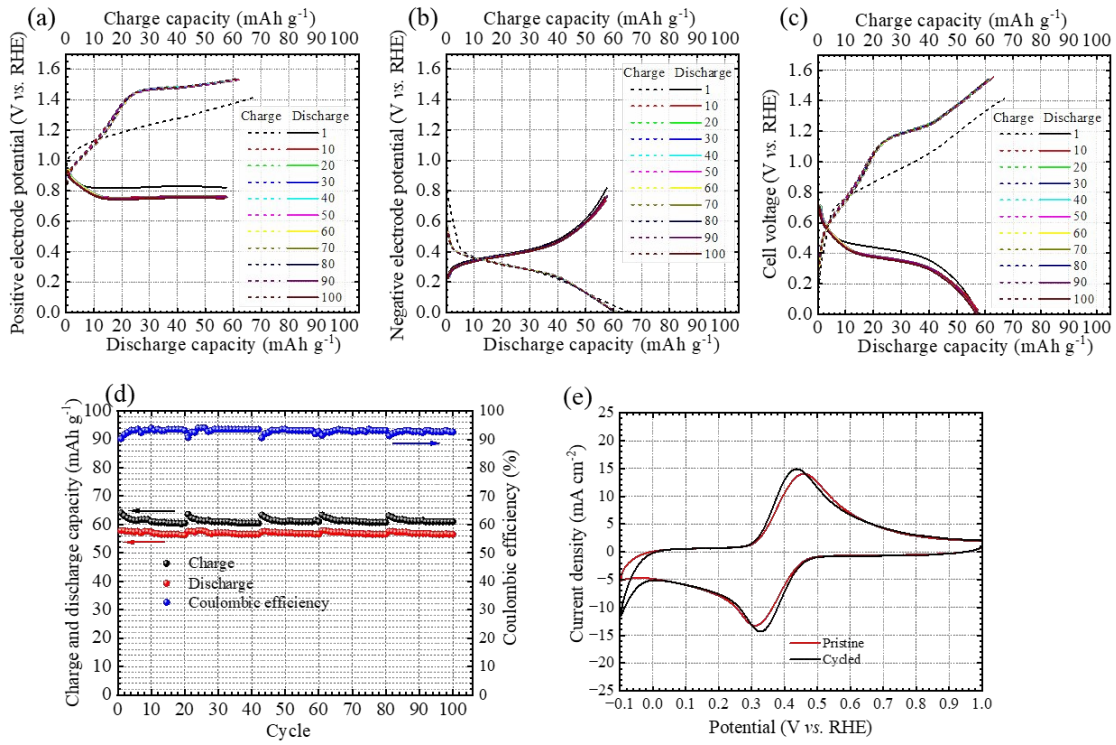

View Article Online
DOI: 10.1039/D5SE00825E

Figure 4. Charging/discharging curves of the SSAB-PPNQ cell measured during cycling at 0.88 mA cm^{-2} (at 15 C rate): (a) positive electrode potential, (b) negative electrode potential, and (c) cell voltage. Changes in (d) charge/discharge capacities and Coulombic efficiencies during cycling. (e) CV curves scanned at 20 mV s^{-1} for pristine and cycled negative electrodes.

Conclusion

We successfully synthesized a novel redox-active NQ-based polymer, PPNQ, and evaluated its electrochemical properties when used as the negative electrode material in an SSAB. To the best of our knowledge, this represents the first demonstration of a polymeric NQ-based material integrated into an all-solid-state air battery system. Compared to previously examined small organic molecules, such as NQ, polymeric PPNQ exhibited enhanced affinity for the hydrophilic proton-conductive polymer (Nafion^{TM}), facilitating proton transport and leading to higher redox-active material utilization, thereby improving the capacitive performance of the SSAB-PPNQ cell. Furthermore, PPNQ functioned more stably in the electrode than other materials, demonstrating reduced dissolution and/or possible degradation during repeated charge/discharge cycles, which enhanced the rate properties (84% retention of its discharge capacity at 100 C) and cyclability (98% retention of its charge/discharge capacities over 100 cycles) of the SSAB-PPNQ cell. This stable performance under high-rate and long-term cycling conditions is particularly notable for an organic polymer in all-solid-state battery configurations. These findings highlight the promising electrochemical performance of PPNQ under reduced humidity conditions and present a new molecular design strategy for organic electrode materials that enables both high stability and excellent redox reversibility. They also underscore the potential of redox-active polymers as efficient and durable electrode materials for high-performance SSABs.

View Article Online
DOI: 10.1039/D5SE00825E

Data availability

The data supporting this article has been included as part of the ESI.

Conflicts of interest

There are no conflicts of interest to declare.

Author contributions

Lin Guo: Investigation and writing. Kenji Miyatake: Supervision, writing, reviewing and editing, funding acquisition, and project administration. Fang Xian: Reviewing. Fanghua Liu: Reviewing. Ahmed Mohamed Ahmed Mahmoud: Reviewing. Vikrant Yadav: Reviewing. Chun Yik Wong: Reviewing.

Acknowledgements

This work was partly supported by the Ministry of Education, Culture, Sports, Science and Technology (MEXT), Japan, through Grants-in-Aid for Scientific Research (23H02058) and MEXT Program: Data Creation and Utilization Type Material Research and Development Project (JPMXP1122712807), and JKA promotion funds from AUTORACE.

References

1. Q. Sun, L. Dai, T. Luo, L. Wang, F. Liang and S. Liu, *Carbon Energy*, 2022, **5**.
2. Y. Sun, *ACS Energy Lett.*, 2020, **5**, 3221-3223.
3. H. Wan, Z. Wang, W. Zhang, X. He and C. Wang, *Nature*, 2023, **623**, 739-744.
4. J. Sung, J. Heo, D. Kim, S. Jo, Y. Ha, D. Kim, S. Ahn and J. Park, *Mater. Chem. Front.*, 2024, **8**, 1861-1887.
5. G. Cong, W. Wag, N. Lai, Z. Liang and Y. Lu, *Nat. Mater.*, 2019, **18**, 390-396.
6. P. Leung, D. Aili, Q.Xu, A. Rodchanarowand and A. A. Shah, *Sustain. Energy Fuels*, 2018, **2**, 2252-2259.
7. S. Li, S. Hu, H. Li and C. Han, *Angew. Chem. Int. Ed.*, 2024, **63**, e202318885.
8. K. Oka, S. Murao, M. Kataoka, H. Nishide and K. Oyaizu, *Macromolecules*, 2021,

View Article Online
DOI: 10.1039/D5SE00825E

54, 4854-4859.

9. L. Zhong, Z. Fang, C. Shu, C. Mo, X. Chen and D. Yu, *Angew. Chem. Int. Ed.*, 2021, **60,** 10164-10171.
10. M. Yonenaga, Y. Kaiwa, K. Oka, K. Oyaizu and K. Miyatake, *Angew. Chem. Int. Ed.*, 2023, **62**, e202304366.
11. K. Miyatake, S. Wada, L. Guo, F. Xian, F. Liu, A. M. A. Mahmoud, V. Yadav and C. Y. Wong, *Energy Environ. Mater.,* 2025, **8**, e12887
12. L. Zhao, Y. Li, M.Yu, Y. Peng and F. Ran, *Adv. Sci.*, 2023, **10**, 2300283
13. L. Guo, K. Miyatake, S. Wada, K. Oka, S. Kitajima, H. Kasai, R. Tanaka, H. Imoto, K. Naka, F. Xian, F. Liu, A. Mohamed Ahmed Mahmoud, V. Yadav and C. Y. Wong, *ACS Sustainable Chem. Eng.*, 2024, **12**, 16518−16523
14. A. Rana, K. Roy, J. N. Heil, J. H. Nguyen, C. Renault, B. M. Tackett and J. E. Dick, *Adv. Energy Mater.*, 2024, **14**, 2402521

View Article Online
DOI: 10.1039/D5SE00825E

The data supporting this article have been included as part of the Supplementary Information.

View Article Online
DOI: 10.1039/D5SE00825E